



# Rare Earth Element and Yttrium Partitioning in Modern Microbialites from Lake Eyasi, Tanzania

*Jackson Vaughn*

B.Sc. Thesis Earth and Environmental Sciences

Thesis Supervisor: Prof. Dr. M. Bau

Second Reviewer: Dr. T. Kreitsmann

June 27, 2025



## Statutory Declaration

Family Name, Given/First Name	<i>Vaughn, Jackson</i>
Matriculation number	<i>30004076</i>
What kind of thesis are you submitting: Bachelor-, Master- or PhD-Thesis	<i>Bachelor-Thesis</i>

### English: Declaration of Authorship

I hereby declare that the thesis submitted was created and written solely by myself without any external support. Any sources, direct or indirect, are marked as such. I am aware of the fact that the contents of the thesis in digital form may be revised with regard to usage of unauthorized aid as well as whether the whole or parts of it may be identified as plagiarism. I do agree my work to be entered into a database for it to be compared with existing sources, where it will remain in order to enable further comparisons with future theses. This does not grant any rights of reproduction and usage, however.

The Thesis has been written independently and has not been submitted at any other university for the conferral of a PhD degree; neither has the thesis been previously published in full.

### German: Erklärung der Autorenschaft (Urheberschaft)

Ich erkläre hiermit, dass die vorliegende Arbeit ohne fremde Hilfe ausschließlich von mir erstellt und geschrieben worden ist. Jedwede verwendeten Quellen, direkter oder indirekter Art, sind als solche kenntlich gemacht worden. Mir ist die Tatsache bewusst, dass der Inhalt der Thesis in digitaler Form geprüft werden kann im Hinblick darauf, ob es sich ganz oder in Teilen um ein Plagiat handelt. Ich bin damit einverstanden, dass meine Arbeit in einer Datenbank eingegeben werden kann, um mit bereits bestehenden Quellen verglichen zu werden und dort auch verbleibt, um mit zukünftigen Arbeiten verglichen werden zu können. Dies berechtigt jedoch nicht zur Verwendung oder Vervielfältigung.

Diese Arbeit wurde in der vorliegenden Form weder einer anderen Prüfungsbehörde vorgelegt noch wurde das Gesamtdokument bisher veröffentlicht.

June 27, 2025




---

Date, Signature



**Abstract.**

Microbial mats are layers of microbial communities which form structures through complex chemical interactions with their ambient water. After the biofilm has undergone lithification, these structures are called microbialites and are preserved in the rock record. The current precedent among researchers is that these biogenic rocks hold the key to paleo-environmental reconstruction for up to <3.5 Ga. In order to assess the viability of this theory, it is important to understand the relationship between microbialites and their environment. This can be investigated using a variety of methods, including comparing modern microbialites to their ambient environment. This study lays forth multiple theories to explain the chemical relationship between Holocene-aged microbialites from Lake Eyasi, Tanzania and their ambient environment. Possible explanations for the REY patterns (as well as trace and major element compositions) observed in the microbialite rely on the discrimination of trapping and binding processes from processes involving precipitation. The variety of individual morphologies observed within the microbialite(s) is not indicative of varying composition or changes in the predominant formation process. Instead, these variations could be linked to changes in the environment, which in turn influence the microbial communities. The study should act as a stepping off point for future research. If any future analysis necessitates dissolution of a biogenic carbonate matrix, a 0.5 M HNO<sub>3</sub> leaching should be performed for both accuracy and practicality.



## Contents

<b>1</b>	<b>Introduction</b>	<b>5</b>
1.1	Microbialite Formation . . . . .	6
1.2	Geological and Hydrological Setting . . . . .	7
1.3	Aims and Objectives . . . . .	8
<b>2</b>	<b>Methodology</b>	<b>9</b>
2.1	Sampling Methods . . . . .	9
2.2	Sample Digestion and Leaching . . . . .	10
2.3	Analytical Methods . . . . .	12
2.4	Data Analysis . . . . .	12
<b>3</b>	<b>Results</b>	<b>13</b>
3.1	Major Element Composition . . . . .	13
3.2	REY Concentrations . . . . .	13
3.3	Trace and Major Element Correlations . . . . .	17
<b>4</b>	<b>Discussion</b>	<b>18</b>
4.1	Classification . . . . .	18
4.2	Mineralogy . . . . .	19
4.3	Shale-normalized Patterns . . . . .	20
4.4	REY Input-Normalization . . . . .	20
4.4.1	Ambient Water Normalization . . . . .	20
4.4.2	Terrigenous Normalization . . . . .	23
<b>5</b>	<b>Conclusions</b>	<b>26</b>
	<b>References</b>	<b>28</b>
	<b>Appendix</b>	<b>32</b>



## 1 Introduction

REE (rare earth element) geochemistry is commonly used to investigate the petrogenesis of igneous rocks and the mixing of ocean water (e.g., Jakeš and Gill 1970; Elderfield et al. 1988). REEs are useful tracers for geochemical processes thanks to properties explained by the lanthanide contraction. The lanthanide contraction refers to the subsequent decrease in ionic radii with increasing atomic number along the lanthanide series (La to Lu). The increase in atomic number along the series is accompanied by an increase in the effective nuclear charge, thereby pulling the electrons closer and decreasing the radii. This is observed particularly in the lanthanide series because it involves the filling of the 4f electron orbitals, which are unique in their lack of ability to shield other electrons from nuclear charge (Rollinson 1995). The REEs behave so similarly that they are almost inseparable, however slight differences in their geochemical behavior cause fractionation in specific environments. For example, due to size differences, HREEs are preferentially incorporated into rock from the melt. Additionally, because of the redox sensitivity of Ce and Eu, they behave differently in oxidizing and reducing environments, respectively, compared to their consistently trivalent counterparts. When plotting REEs, samples are typically normalized against an REE pattern which represents their source input in order to, among other reasons, remove the effects of Oddo-Harkins rule so that the elements are comparable. This means that deviations in an otherwise flat pattern are indicative of certain processes. REYs (rare earth elements + yttrium) are often plotted together because Y is the geochemical twin of Ho, meaning Y behaves like Ho, with slightly different properties. Comparing Y/Ho ratios adds another opportunity to discern processes which may have influenced a sample.

Microbialites are organosedimentary deposits formed by microbial communities which trap and bind particulate matter found in the ambient water and/or precipitate their structures out of solution (Dupraz et al. 2009). Microbial mats are considered the oldest ecosystems on Earth (Hofmann et al. 1999; Allwood et al. 2007), consisting of layered communities of bacteria involved in complex mineral/water interactions (Dupraz et al. 2009). These microbial mats preserve their structures and potentially chemical information after diagenesis in the form of microbialites (Dupraz et al. 2009; Webb and Kamber 2000; Krumbein et al. 2003). Biogenic stromatolites provide evidence for early life on Earth, preserving signatures of microbial activity up to <3.5 Ga (Hofmann et al. 1999). The current precedent among researchers is that relationships can be derived between modern microbialites and their ambient environment which can subsequently be applied to ancient microbialites to reconstruct their paleo-environment, i.e., ascertain information regarding the chemical environment in which life formed (e.g., Webb and Kamber 2000; Van Kranendonk et al. 2003). In the case of REYs, if microbialites preserve the REY signatures from their ambient environment, this would allow for the reconstruction of paleo-seawater chemistry using REY signatures from ancient stromatolites. However, other researchers have taken the stance that without a holistic understanding of the interactions between microbial mats and their environment, these supposed relationships are unfounded (e.g., Johannesson et al. 2014; Dupraz et al. 2009). This topic remains an important point of contention in the field of paleo-geochemistry.

## 1.1 Microbialite Formation

While the processes involved in the formation of microbial carbonates are still not completely understood, comprehending these processes is crucial to accurately interpret rock records (Dupraz et al. 2009). The most common microbialites are carbonates (Dupraz et al. 2009), which are categorized into four primary macrostructures: stromatolites (laminated), thrombolites (clotted), dendrolites (dendritic), and leiolites (aphanitic) (Riding 2011). Stromatolites are the most widespread and most studied of the microbialites. Stromatolites are laminated benthic microbialites with various individual sub-categorizations relating to structure, which may be a reflection of their formation process (Riding 1991).

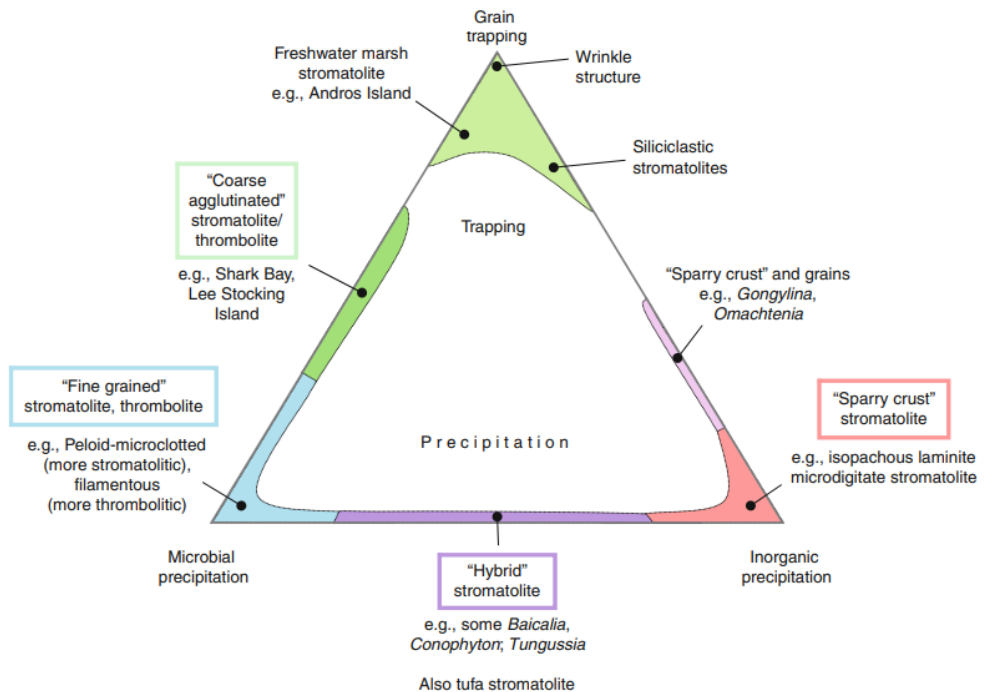


Figure 1: Diagram illustrating the relationship between the microstructures of stromatolitic and thrombolitic morphologies and their respective formation processes. Figure from Riding [2011].

Modern analytical techniques have shown that the variability in bacterial communities within microbial mats should not be underestimated (e.g., White III et al. 2015; Dupraz et al. 2009). Numerous bacterial species play various roles in the formation of microbialites depending on their respective taxonomic functional potentials (Dupraz et al. 2009). The most common microbial communities involved in the formation of microbialites are sulfate reducing bacteria (heterotrophic) and photosynthesizing cyanobacteria (autotrophic) (Dupraz et al. 2009). There are two primary ways in which microbial carbonates are formed: trapping and precipitation. The latter of which can be further subdivided into two categories of organomineralization: biologically-induced and biologically-influenced mineralization (Dupraz et al. 2009). The environmental conditions govern the type and rate of bacterial metabolism as well as the stability and potential for fossilization of the

microbialite (Dupraz et al. 2009). During biologically-induced mineralization, metabolic activity creates microenvironments which are conducive to carbonate precipitation, the efficacy of which is influenced by environmental conditions, namely high pCO<sub>2</sub> and/or increased water alkalinity (Dupraz et al. 2009). The precipitates subsequently act as substrates for further microbial growth, changing the mat properties, and resulting in either negative or positive feedback loops within the ecosystem (i.e., interactions between the microbial mat and its environment will form an environment either conducive or unfavorable to further mat growth) (Dupraz et al. 2009). The precipitation of carbonate minerals during organomineralization is driven by the 'alkalinity engine,' a function of alkalinity and free calcium represented by a saturation index (Dupraz et al. 2009). The alkalinity engine is comprised of intrinsic (microbial metabolism [biologically-induced]) and extrinsic (environment [biologically-influenced]) components (Dupraz et al. 2009). The mineral initially nucleates on the organic matrix, however the shape and composition of the mineral is determined by the EPS (extracellular polymeric substance[s]) matrix (Dupraz et al. 2009). The EPS essentially determines how microbial cell walls interact with their environment. In both cases of organomineralization, the EPS matrix is responsible for the mineralogical composition of the subsequent microbialite. With regards to REY geochemistry, it is vital to understand if the EPS matrix results in the fractionation of REYs during carbonate precipitation. If so, then this severely limits the potential to derive accurate information from ancient stromatolites regarding their paleo-environment.

## 1.2 Geological and Hydrological Setting

Lake Eyasi is situated in a graben rift basin within the East African Rift System (Deocampo 2005), an area subject to large-scale extensional block faulting (Dawson et al. 1994). The area is comprised of primarily igneous rocks ranging from trachytic and basaltic lavas to trachyandesitic and carbonatitic ashes from Pliocene to Quaternary volcanic activity (Dawson et al. 1994). Lake input primarily consists of fluvial drainage from the Serengeti (in the northwest) and elevated metamorphic highlands (in the southeast) (Deocampo 2005). The lake margin consists of various points of groundwater discharge associated with locally-stromatolitic travertines which have coated the Oldeani volcanics (Deocampo 2005; Casanova 1994). The East African Rift System includes a number of soda lakes, including Lake Eyasi. Soda lakes are saline and alkaline lacustrine environments where speciation of dissolved ions consists of predominately carbonate and sodium species (Deocampo and Renaut 2016). These seasonal lakes evolve an evaporative brine as they are situated in hydrologically closed basins with dilute alkaline inflow (Deocampo and Renaut 2016). The alkalinity is caused by the silicate hydrolysis of weathered volcanic material (Deocampo and Renaut 2016). Since dilute inflow has a positive bicarbonate to calcium ratio, Ca and Mg are removed during early brine evolution with the precipitation of calcium carbonate, leaving Na as the predominant dissolved cation in the East African Rift soda lakes (Deocampo and Renaut 2016). Ergo, groundwater input is often a pre-requisite for the continued formation of carbonates in soda lakes (Deocampo and Renaut 2016).

### 1.3 Aims and Objectives

This study evaluates locally formed Holocene-aged stromatolitic microbialites from Lake Eyasi, Tanzania in the context of their ability to represent the REY geochemistry of their ambient environment. Few studies have investigated the REY signature of terrestrial microbialites with respect to that of their ambient environments. The intent here is to categorize the stromatolites in order to better understand the process(es) in which they were formed. This knowledge is then utilized to apply context to a comparison of the REY signatures of the microbialites and their ambient water. Contextualizing the relationship between the two could provide further insight into the potential for using ancient stromatolites as paleo-environmental proxies. The potential for EPS to fractionate REYs during precipitation is investigated by plotting the microbialites REY concentrations against those of their ambient water, and subsequently calculating the "solid-liquid partitioning coefficients" between the two. Furthermore, different sections within the microbialite are compared to test for differences in trace and/or major element composition, which could have implications on the formation processes surrounding different microbialite morphologies. Additionally, the trace and major element compositions of the microbialites are compared to those of their pore material, their ambient detritus, and their ambient water. Different digestion/leaching methods are also tested to investigate the pros and cons of extraction methods for future analysis of biogenic carbonates.

## 2 Methodology

### 2.1 Sampling Methods

In the Summer of 2022, Professor Dr. Michael Bau and Dr. Timmu Kreitsmann took samples from the Eastern side of Lake Eyasi, Tanzania. Water and microbialite samples were analyzed in the geochemistry lab at Constructor University by Timmu Kreitsmann and Jackson Vaughn, respectively.

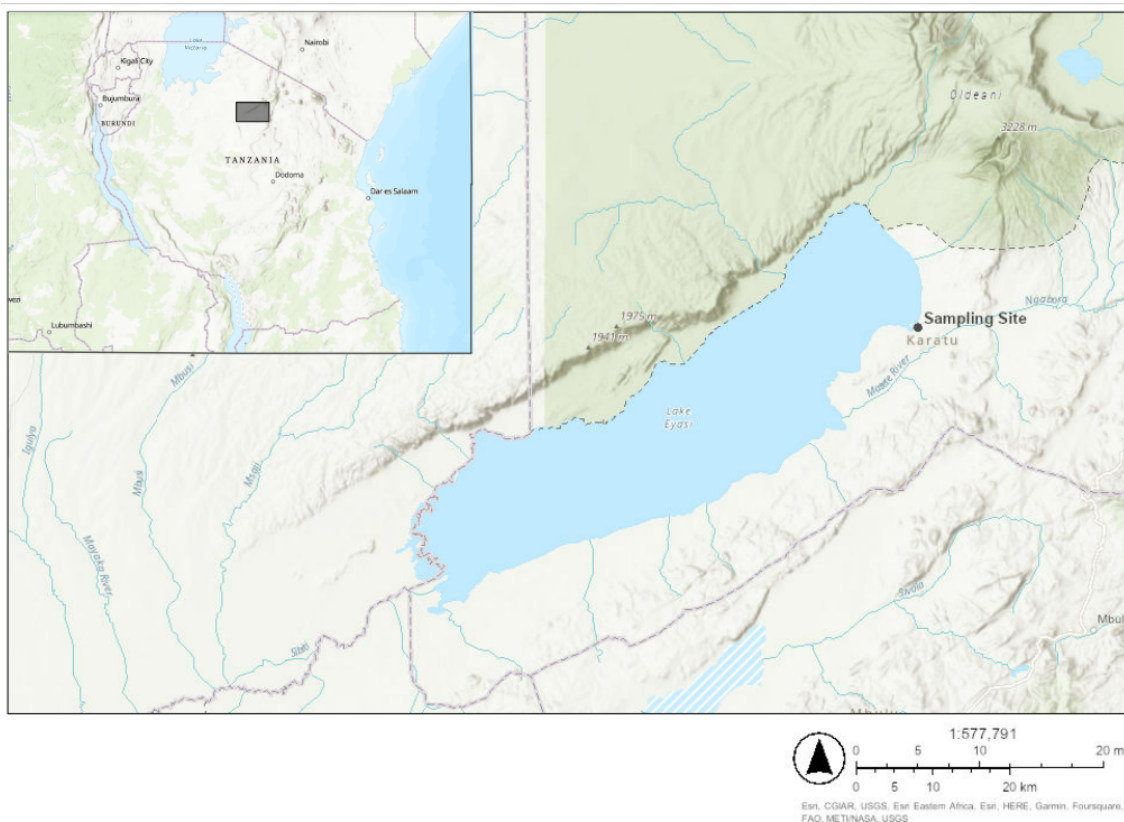


Figure 2: Map of Lake Eyasi, Tanzania with the sampling site depicted (latitude -3.498889 and longitude 35.346389) produced using ArcGIS Online.

Of the collected microbialite samples, 11 samples were derived from different areas within the microbialite (Figure 4). At Constructor University, samples 1-6 were isolated using the lapidary trim saw, whereas samples 7-10 were taken using the 5 mm microdrill. Sample 11 was taken by scraping out sediment which had accumulated within the pores of the microbialite.



Figure 3: Picture of the microbialite on the field with a key for size reference, photo: T. Kreitsmann.

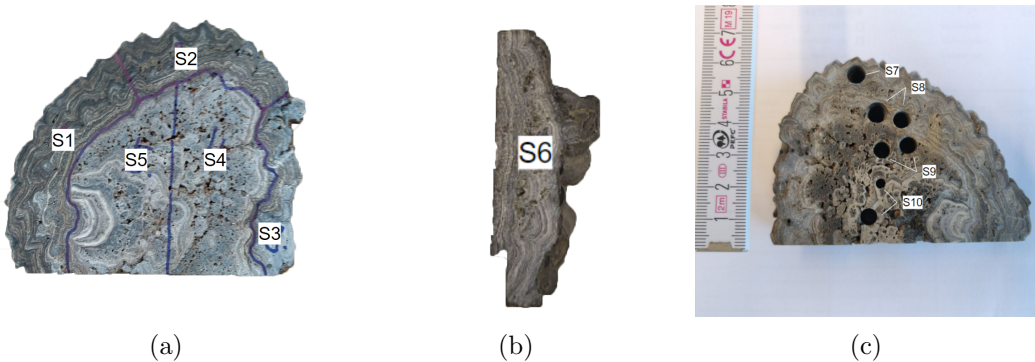


Figure 4: Panel (a) depicts the microbialite divided into sections 1-5. Panel (b) displays sample 6, taken from the outermost layer of the microbialite. Panel (c) shows drill holes where microbialite samples 7-10 were taken from.

## 2.2 Sample Digestion and Leaching

In the Constructor University Geochemistry Lab, ICP-MS (inductively coupled plasma mass spectrometry) is used to determine trace element concentrations of the microbialite samples, while OES (optical emission spectrometry) is used for determining major element composition. ICP-MS and OES require dissolution of the carbonate matrix in order to free trace elements from the mineral phase to make them available for analysis. Microbialite samples S1-S5 are each digested/leached using four different procedural methods, with each method correlating to a different job number (68, 78, 80, 06)(Table 1). Samples S6-S10 are each leached using only one method associated with job number 12. Sample 11 was digested using methods associated with job numbers 12 and 14. All samples were crushed into finely grained powder using an agate mortar and pestle. Filter syringes used in the digestion process were first cleaned by filtering 0.1 M HNO<sub>3</sub> once through and subsequently deionized water (DI) three times through the filter membrane. During each digestion procedure,

CRMs (certified reference material) and a method blank were prepared alongside the samples. Digested samples are labeled according to their respective sample and job number (e.g. S1-68).

Table 1: Digestion/leaching methods

Job Number:	68+14	78	80	06+12
Extraction Method:	HCl+HNO <sub>3</sub> +Hf	5 M HNO <sub>3</sub>	5% CH <sub>3</sub> COOH	0.5 M HNO <sub>3</sub>

Jobs 68 and 14 consisted of a bulk digestion of samples according to procedure from Schier et al. [2021]. 0.25 g of the samples and CRM (JLs-1 [Japanese-limestone]) were measured and placed in the oven to dry overnight at 105 °C. Samples were subsequently dissolved in an acid mixture consisting of suprapure concentrated 3 ml HCl, 1 ml HNO<sub>3</sub>, and 1 ml HF at 165 °C for 16 hours using PicoTrace high-temperature high-pressure digestion system. The acid-sample mixture was then evaporated twice through the addition of 5 ml suprapure concentrated HCl followed by dissolving the mixture an additional time in 0.5 M HNO<sub>3</sub>. During the digestion of samples in job 68, a white precipitate formed. In order to isolate the supernatant, samples were filtered into PE bottles through 0.2 µm syringe filters where 0.5 M HNO<sub>3</sub> was added until the total volume reached 50 ml.

Job 78 consisted of leaching samples following another method provided by Schier et al. [2021]. 0.25 g of each sample and CRM (JLs-1) were placed in the oven to dry at 105 °C overnight. 0.15 g of CRM BEAN was also included. The dried samples were then dissolved using 10 ml of 5 M HNO<sub>3</sub> in open beakers and subsequently evaporated to dryness. After which 0.5 M HNO<sub>3</sub> was added to the samples and left to cool at room temperature. Samples were then filtered through a 0.2 µm membrane into PE bottles. Finally, 0.5 M HNO<sub>3</sub> was added until the total volume reached 50 ml.

Job 80 consisted of leaching samples in accordance with the procedural method suggested by Rongemaille et al. [2011]. 0.05 g of each sample and CRM (JLs-1 and BEAN) was measured and placed in the oven overnight to dry at 105 °C. Afterwards 6 ml of 5% acetic acid (CH<sub>3</sub>COOH) was added to the sample. The acid-sample mixture was left to sit for 24 hours before centrifugation (2min/2500rpm). The supernatant was subsequently filtered through a 0.2 µm membrane into PE bottles. Afterwards, the leachate was evaporated using PicoTrace in order to remove the acetic acid. Finally, 0.5 M HNO<sub>3</sub> was added until the total volume reached 20 ml.

Jobs 06 and 12 consisted of leaching the samples. 0.05 g of each sample and CRM (JLs-1 and BEAN) were measured and placed in the oven to dry overnight at 105 °C. Samples were transferred to precleaned ICP-MS tubes and 10 ml 0.5 M HNO<sub>3</sub> was added. The tubes were shaken slowly with the caps on. After being left overnight under the hood with the caps off, the solutions were filtered through 0.2 µm membrane syringe filters. After which, 0.5 M HNO<sub>3</sub> was added until the tubes were filled to a total volume of 20 ml.

### 2.3 Analytical Methods

CRMs are used in analysis to validate the accuracy of the results. For ICP-MS and OES analysis of samples 1-5 the CRMs used are BEAN and JLS-1, respectively. For ICP-MS and OES analysis of samples 6-11 the CRMs used are JD-1 (Japanese-dolostone) and JLS-1, respectively. For details regarding BEAN refer to Barrat et al. [2020]. For details regarding JLS-1 and JD-1 refer to Dulski [2007].

An internal standard of known composition is added to each sample to account instrumental drift (for detailed information see Alexander [2008]). For ICP-MS 0.06 g of internal standard (100 ppb of Ru-Rh-Re-Bi) is added for each sample. 0.12 g of sample solution is used, then 0.5 M HNO<sub>3</sub> is added until the total volume is 6 g (or until the internal standard has been diluted by a factor of exactly 100). For CRMs 0.24 g of sample is used.

For OES, 0.5 g of a 10 ppm Yttrium stock solution was used as the internal standard. A total of 6 calibration standards were made. Each calibration standard contained a different concentration of the in-house carbonate rock, with the dilution factors being 400, 200, 80, 20, 8, and 4, respectively. The method and control blanks both contained sample diluted to a factor of 3, while the acid blank contained no sample. Each of the aforementioned in-house carbonate rocks were filled to a total volume of 50 ml with 0.5 M HNO<sub>3</sub> diluent. Microbialite samples 6-11 were analyzed with each sample having been diluted to a factor of 6. Microbialite samples 1-5 were analyzed using OES twice, once with each sample being diluted to a factor of 6 and once to a factor of 3.

### 2.4 Data Analysis

The following section consists of the experimental results of OES and ICP-MS analysis, and displays only relevant major and trace element data. For the complete data sets, see the Appendix on page 32. ICP-MS and OES data are evaluated through Excel files provided by the geochemistry lab. Trace element data below the limit of quantification (LOQ) is filtered out, and the remaining REY data is plotted through the use of Python scripts. The LOQ is defined as ten times the standard deviation of the acid blank. Partition coefficients of REYs between the biogenic carbonate and the ambient water is calculated through the use of Python scripts and excel files. REY data is normalized to ELF (Eyasi Lake Filter) data provided by Dr. Kreitsmann, ELW (Eyasi Lake Water) data provided by Dr. Kreitsmann, and PAAS (Post Archean Australian Shale) data published by McLennan [1989]. Samples are here normalized to PAAS to maintain consistency with other microbialite and carbonate REY studies (e.g., Johannesson et al. 2014; Kaya et al. 2023; Webb and Kamber 2000; Johannesson et al. 2006), so that results are visually comparable.

### 3 Results

#### 3.1 Major Element Composition

Table 2: OES data for samples 2, 3, 4, 5, and 11 in percent by weight.

% wt.	Sample 2	Sample 3	Sample 4	Sample 5	Sample 11 (L)	Sample 11 (B)
Al	0.288	0.533	0.304	0.266	1.858	4.950
Ca	34.604	31.252	34.169	34.997	11.918	13.460
Fe	0.091	0.148	0.095	0.082	0.500	4.137
K	0.019	0.027	0.017	0.017	0.079	1.163
Mg	0.486	0.482	0.521	0.511	0.412	1.235
Mn	0.056	0.124	0.053	0.054	0.072	0.126
Na	0.835	0.960	0.859	0.782	2.345	3.553
Sr	0.687	0.606	0.729	0.760	0.243	0.261

(L) is the leaching and (B) is the bulk digestion.

Table 2 shows the major element composition of specific microbialite sections. Samples 2-5 use data from 0.5 M HNO<sub>3</sub> leachings, whereas sample 11 uses data from both a 0.5M HNO<sub>3</sub> leaching as well as a bulk digestion. When comparing the leaching and bulk digestion results of sample 11, there is a pronounced disparity between concentrations of almost every major element. Sample 11 is likely not a carbonate since the leaching was unable to dissolve much of the matrix. With the exception of Sr, the concentrations measured from the bulk digestion are significantly higher than those measured from the leaching. As expected, samples 2-5 are similar with sample 11 being the outlier. Due to the microbialite's carbonate matrix, samples 1-10 were easily dissolved by the 0.5 M HNO<sub>3</sub> leaching. There is little disparity between the digestion and leaching results of the microbialite samples. Among samples 2-5, sample 3 stands out for it's elevated concentrations of Al, Fe, K, Mn, and Na, while displaying lower concentrations of Ca and Sr. The uniqueness of sample 3 is consistent across other extraction methods. Sample 11 exhibits a radically different major element composition. Nonetheless, the concentrations of elements in sample 11 relative to sample 2, 4, and 5, follow the same pattern as sample 3 to a greater scale.

#### 3.2 REY Concentrations

In Figure 5 each method results in approximately the same pattern, with the exception of the bulk digestion which resulted in depleted Y levels and overall lower REY concentrations. Since each leaching method results in approximately the same concentrations, the following figures will focus on data from the 0.5M HNO<sub>3</sub> leaching as it is the method most easily reproduced. However, this only applies to the carbonate samples. As sample 11 is not a carbonate, the subsequent plots will utilize the bulk digestion for sample 11 specifically.

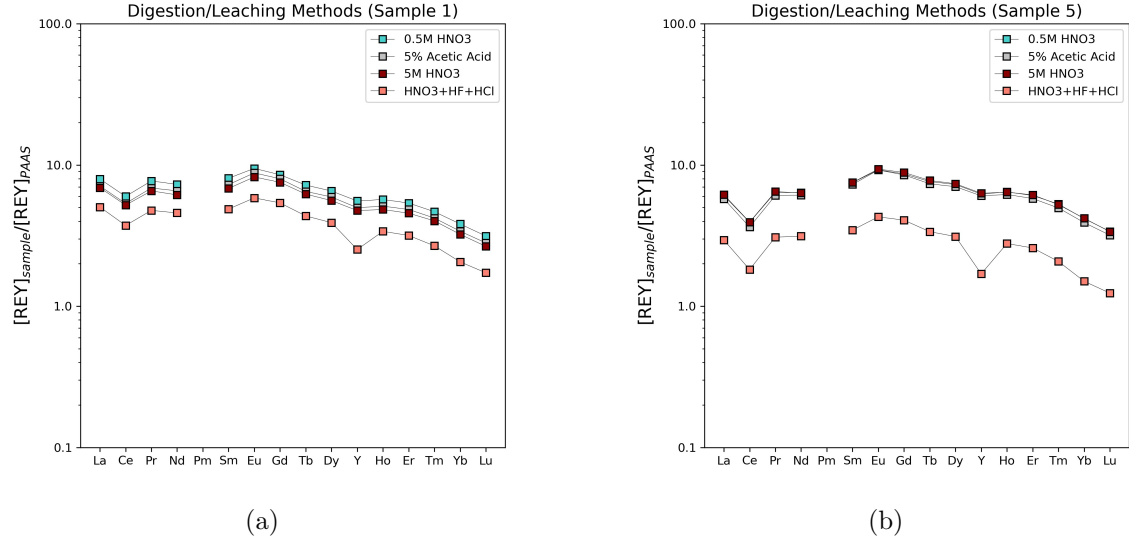


Figure 5: Panel (a) and panel (b) display the REY patterns of samples 1 and 5 prepared using each of the aforementioned extraction methods.

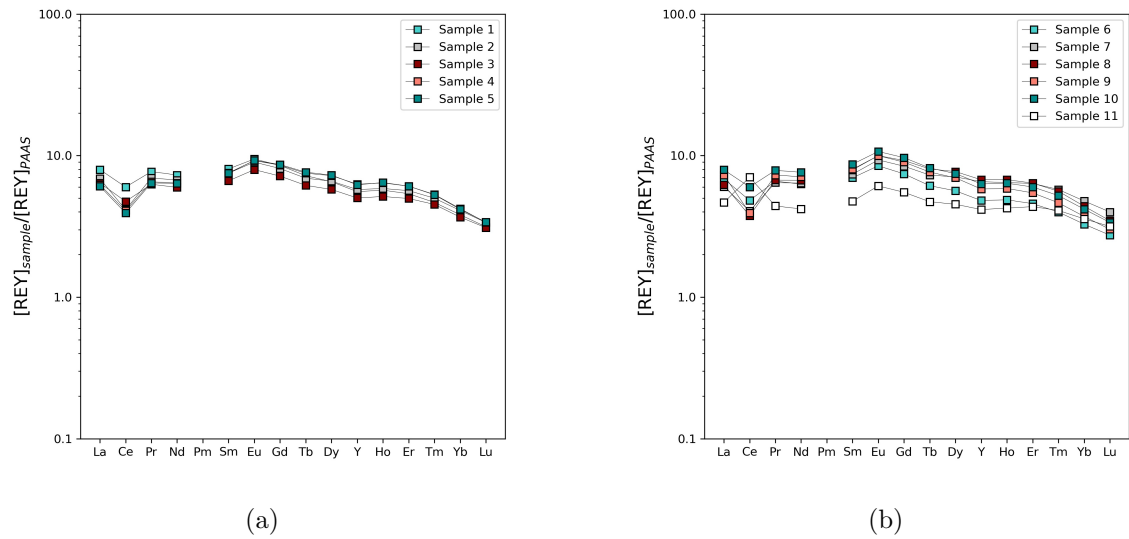


Figure 6: Panel (a) and panel (b) show all microbialite samples normalized to PAAS.

In Figure 6, panel (a) and panel (b) illustrate a consistent REY pattern across samples 1-10. Sample 11 conversely contains a positive Ce anomaly, and is further depleted in LREEs than samples 1-10.

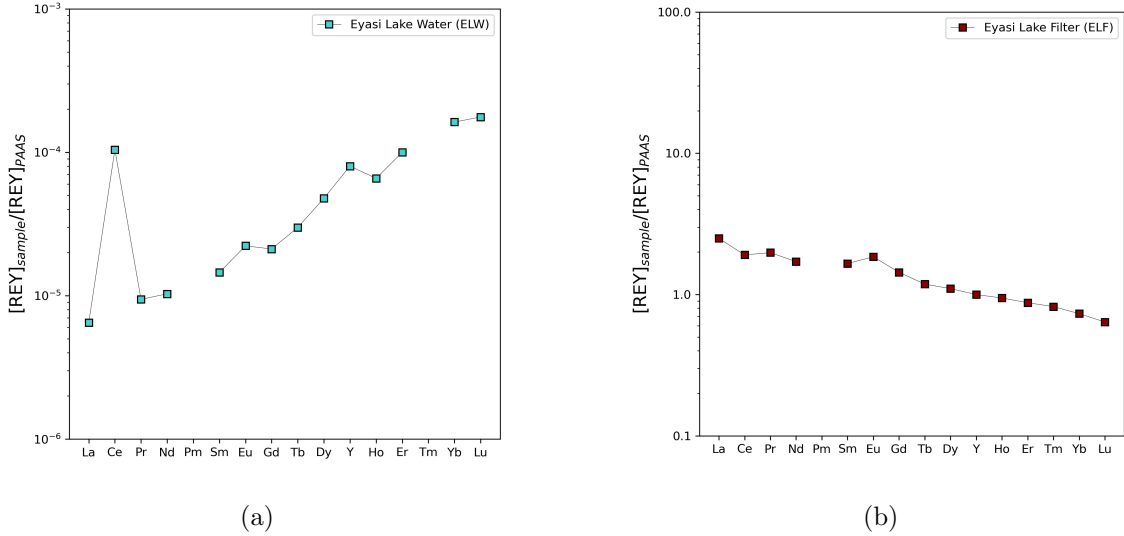


Figure 7: Panel (a) and panel (b) show the REY patterns of a ELW and ELF, respectively. ELF data represents the terrigenous fraction, as it is the detritus filtered out of the ambient lake water (i.e. particulates  $>0.2 \mu\text{m}$ ).

Figure 7b shows ELF to be depleted of HREEs when normalized to PAAS. By contrast, ELW in Figure 7a displays a significant depletion of LREEs and corresponding enrichment of HREEs. Both patterns show a minor positive Eu anomaly. The ELF pattern shows what could be considered a minor negative Ce anomaly, however the ELW pattern displays a major positive Ce anomaly. The Y/Ho ratios of ELW and ELF are 33.174 and 28.853, respectively. The Yb/Nd ratios of ELW and ELF are 0.428 and 0.992, respectively.

Table 3 presents the REY concentrations across all sections of the microbialite. Results for sample 11 are displayed twice, once for the bulk digestion and once for the leaching. The bulk digestion method reveals consistently higher concentrations of elements in sample 11. Results do not tend to vary between sections, except in the case of sample 11. Element concentrations for sample 11 are significantly lower than every other sample, with the exception of Ce which is higher. Sample 10 also contains a relatively high concentration of Ce, although still lower than sample 11. Additionally, table 3 presents the respective Y/Ho and Yb/Nd<sub>SN</sub> ratios for each microbialite sample. The Y/Ho ratios remain constant at around 26 across all samples, with the exception of the sample 11 leaching. The Yb/Nd<sub>SN</sub> ratios are relatively constant around 0.6 across samples 1-10, however sample 11 is slightly higher at just under 0.9.

### 3 RESULTS

Table 3: REY concentrations for samples 1-10 using 0.5M HNO<sub>3</sub> leaching, and sample 11 using a bulk digestion.

mg/kg	Sample 1	Sample 2	Sample 3	Sample 4	Sample 5	Sample 6	Sample 7	Sample 8	Sample 9	Sample 10	Sample 11 (leach)	Sample 11 (bulk)
La	304.205	262.746	244.549	237.960	232.118	261.718	230.449	237.713	278.410	303.054	153.609	178.007
Ce	477.116	329.738	377.458	324.181	312.751	383.704	323.354	299.192	313.435	477.604	511.935	560.051
Pr	67.853	61.235	55.154	57.455	56.375	58.046	56.702	59.103	64.156	69.238	32.862	38.772
Nd	247.145	227.351	202.285	217.151	215.867	213.367	216.630	226.739	240.201	258.275	119.469	142.385
Sm	44.699	41.709	36.812	41.882	41.678	38.675	41.013	43.999	44.432	48.237	22.181	26.414
Eu	10.218	9.711	8.593	9.960	9.980	9.146	10.068	10.794	10.785	11.549	5.418	6.594
Gd	39.741	37.768	33.385	39.860	40.298	34.613	39.204	43.015	41.893	45.051	21.428	25.652
Tb	5.579	5.358	4.769	5.810	5.910	4.742	5.639	6.231	5.921	6.321	3.060	3.655
Dy	30.612	30.881	26.980	33.786	34.050	26.388	33.089	36.091	32.614	34.024	18.221	21.202
Y	150.174	155.427	135.504	169.440	167.883	129.919	176.703	182.203	156.684	170.192	98.688	112.248
Ho	5.647	5.801	5.095	6.357	6.393	4.829	6.390	6.697	5.811	6.323	4.219	4.219
Er	15.326	16.123	14.183	17.330	17.330	13.034	18.117	18.221	15.538	17.104	10.883	12.426
Tm	1.890	2.024	1.830	2.151	2.141	1.617	2.332	2.267	1.879	2.113	1.474	1.659
Yb	10.779	11.547	10.360	11.902	11.768	9.239	13.474	12.372	10.477	11.798	8.725	10.076
Lu	1.360	1.458	1.340	1.460	1.467	1.186	1.730	1.501	1.306	1.460	1.154	1.368
(Y/Ho)	26.594	26.792	26.598	26.654	26.262	26.904	27.653	27.205	26.961	26.916	23.391	26.605
(Yb/Nd) <sub>SN</sub>	0.524	0.611	0.616	0.659	0.655	0.521	0.748	0.656	0.524	0.549	0.878	0.851
<i>SN</i> shale-normalized												

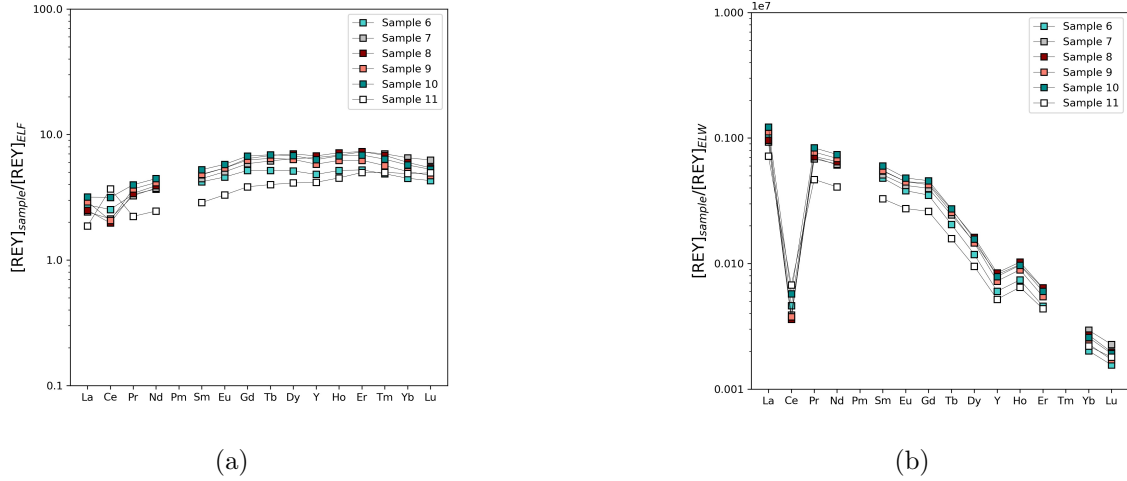


Figure 8: Panels (a) and (b) show samples 6-11 normalized to the REY concentrations of the terrigenous fraction and the microbialite's ambient water, respectively.

When observing the ratio of REY concentrations in the microbialite over the ambient water, Figure 8b depicts a stark contrast between HREE and LREE ratios. The plots reveal a significant enrichment of HREEs and depletion of LREEs within the microbialite with respect to its aqueous surroundings. The plots are additionally characterized by distinct negative Ce anomalies, and higher Y/Ho ratios.

### 3.3 Trace and Major Element Correlations

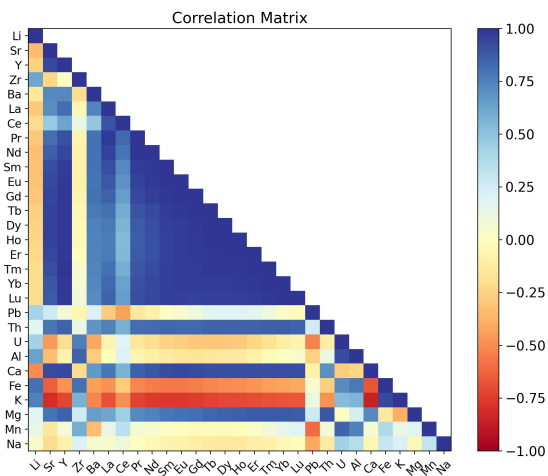


Figure 9: Correlation coefficient matrix of trace and major elements within sections 1-5 of the microbialite.

Figure 9 displays the correlation coefficients between elements both trace and major, indicating the phases in which these elements are bound and highlighting other relationships. Naturally, the REYs correlate nicely with one another, featuring a discernible Ce anomaly. The REYs display a strong positive correlation with Th, Ce, and Mg. Conversely, they display a strong negative correlation with Fe and K.

## 4 Discussion

### 4.1 Classification

Further investigation of the Lake Eyasi microbialites, reveals that they are composite microbialites, more specifically thrombolitic-stromatolites (Riding 2011). The microbialites consist of a finely grained matrix with intermittently scattered coarse grain clasts (<2mm). The microbialite pictured in Figure 10 displays thrombolitic-stromatolitic upward association, with a transitional morphology in-between. (For the remainder of this paper, the microbialites will be referred to as simply stromatolites.)

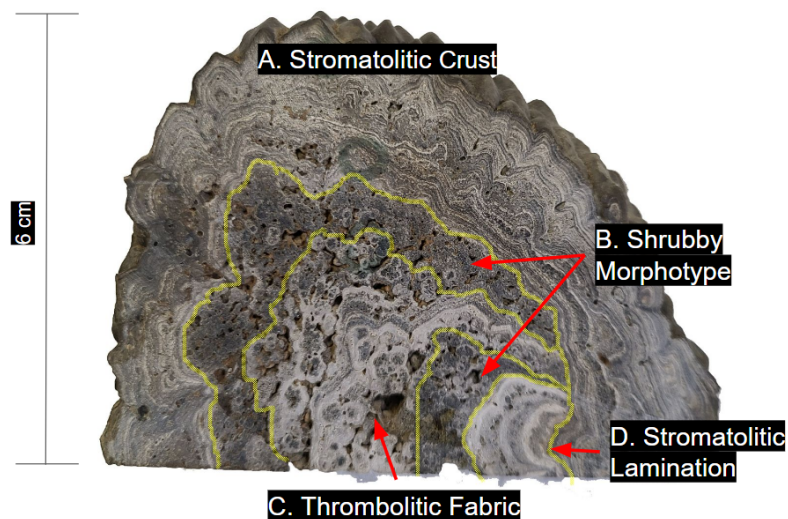


Figure 10: Mesostructures of a Lake Eyasi Stromatolite are demarcated by yellow lines. Section A. is the outermost layer of the stromatolite and consists of wavy stromatolitic lamination, alternating between dark and light gray layers. Section B. consists of a dark gray shrubby morphotype, neither stromatolitic nor thrombolitic, with many small pores. Section C. is comprised of lighter gray clotted thrombolitic fabric with large pore spaces. Section D. appears to be stromatolitic lamination, however the coloration and thickness resemble more so that of the thrombolitic section.

The stromatolite layer, Figure 10 A., is characteristic of a fine grained well laminated agglutinated stromatolite (Riding 1991). The stromatolites display crinkly lamination with fenestrae, typical for stromatolites located in lake margins due to exposure and desiccation (Riding 1991). The Lake Eyasi stromatolites are remarkably similar in morphology to the microbialite studied by Lencina et al. [2021], both of which formed in seasonal saline and alkaline lakes. Lencina et al. [2021] contributes the shift in morphology within the individual microbialite to seasonal variations in water-level and other environmental parameters, which may have led to changes in the composition of microbial communities.

## 4.2 Mineralogy

In Figure 9 it is clear by their correlation with Ca and Mg, that the REYs are bound in the carbonate phase. This is further supported by the Sr concentrations of sample 11 provided in Table 2. Since the leaching primarily targets the carbonate phase, the fact that Sr levels are only slightly higher in the bulk digestion suggests that Sr, an element with geochemical behavior similar to the REYs, is trapped in a carbonate phase. This is confirmed in Table 3, where REY concentrations in sample 11 barely increase from the leaching to the bulk digestion. The close association of Th with the REYs is an indication that the source of the REYs could be terrigenous, since Th is not mobile in aqueous phases in Earth's surface waters (Corkeron et al. 2012). Ergo, no authigenic Th mineral should be able to precipitate from solution. Nonetheless, the solubility of Th is increased in alkaline waters by the presence of carbonate species, meaning we cannot yet rule out this possibility (Östhols 1994). This is not applicable if bicarbonate is the dominant species, which is the case for certain lakes along the East African Rift System. Th shows a negative correlation with elements typically enriched in terrigenous phases (K, Al, Fe) and a positive correlation with elements in authigenic phases (Ca, Sr, REE), which supports the idea of an authigenically precipitated Th mineral. The correlation with Th could be interpreted as contamination from clays, however the negative correlation between REYs and Al, Ca, and K indicate that the results are not contaminated by an aluminosilicate phase.

The consistency of REY data across different leaching methods depicted in Figures 5a and 5b serves as evidence for analytical precision. When preparing samples 1-5 of the bulk digestion for ICP-MS analysis, it was noticed that within the samples some small white crystals had been precipitated. This could account for the lower REY concentrations and negative Y anomaly, as the ICP-MS would not be able to detect any REYs bound within the precipitate phase. The precipitates are most likely calcium fluoride crystals, as the addition of HF may have caused the solution to become supersaturated with respect to  $\text{CaF}_2$ . No other extraction method utilized HF, and no other method formed a precipitate. Since sample 11 is not a carbonate, it does not face the same issue. The bulk digestion allows for both OES and ICP-MS analysis to detect higher concentrations of every element in sample 11 (Table 2 & Table 3).

### 4.3 Shale-normalized Patterns

It is clear from Figure 6 that the various sections of the stromatolites show negligible differences in REY signatures, with the exception of the pore material (sample 11). This indicates that despite different morphologies, which could have been caused by different bacterial species and/or environmental conditions, the principal source(s) and mechanism(s) for REE uptake remained the same throughout its lifetime. Differences in the major element compositions of different sections within the stromatolites are characterized by certain sections resembling sample 11 more than others, namely sample 3. This is likely due to contamination from pore material caused by increased porosity in certain sections.

The PAAS normalized REY patterns of the modern Lake Eyasi stromatolites depicted in Figure 6 are distinct from the typical literature values for a stromatolite. Stromatolite samples 1-10 are depleted in HREEs, with  $\text{Yb}/\text{Nd}_{\text{SN}}$  values which range from  $\sim 0.52$  to  $0.75$  [mean  $\text{Yb}/\text{Nd}_{\text{SN}}$  ( $\pm \text{SD}$ ) =  $0.606 \pm 0.104$ ]. A stark contrast in comparison to the, also terrestrial, HREE enriched Cuatro Ciénelas stromatolites [mean  $\text{Yb}/\text{Nd}_{\text{SN}}$  ( $\pm \text{SD}$ ) =  $1.13 \pm 0.16$ ] cited by Johannesson et al. [2014]. The Lake Eyasi stromatolite additionally does not feature the negative Eu anomaly seen in the Cuatro Ciénelas stromatolites from Johannesson et al. [2014], rather a negative Ce anomaly.

### 4.4 REY Input-Normalization

#### 4.4.1 Ambient Water Normalization

Claims that microbialites can be used as a proxy for the REY signatures of their ambient water (e.g., Allwood et al. 2007), operate on the grounds that modern microbialites do not fractionate REYs. If this is the case, then modern microbialites would show uniformly flat REY patterns when normalized to their ambient water. However, as evident by Figure 8b, this is not the case for the Lake Eyasi stromatolites.

Assuming that the stromatolite's ambient water is its primary source of REYs, then the ambient water normalized REY patterns are comparable to solid-liquid partitioning coefficients (e.g., Johannesson et al. 2014, Takahashi et al. 2005). This comparison does not apply to stromatolites which formed by trapping and binding detrital sediment. Currently, it remains difficult to discriminate between stromatolite formation processes post-mortem, despite assertions that trace element (REY+Th) geochemistry can be used for this purpose (e.g., Corkeron et al. 2012). In order for the ambient water to be the stromatolites primary source of REY's, the stromatolite must be precipitated out of solution. Among the stromatolites which are precipitated, there remains two primary subgroups, those which are microbially precipitated and those which are inorganically precipitated (Riding 2011). The former can be further subdivided into biologically-induced and biologically influenced, as previously discussed. The distinction between these should be made when possible, because the different processes may reflect their REY source differently i.e. fractionate REYs in different ways.

Table 4: Solid-liquid distribution/partitioning coefficients for Lake Eyasi and Cuatro Ciénegas stromatolites, and Nakabusa hot spring microbialites.

	Samples 1-10 <sup>a</sup> ( $\times 10^3$ )	Sample 11 <sup>a</sup> ( $\times 10^3$ )	Rio Mesqu- ites <sup>b</sup> ( $\times 10^3$ )	El Mojarrel West <sup>b</sup> ( $\times 10^3$ )	Sample 1 <sup>c</sup> ( $\times 10^3$ )	Sample 2 <sup>c</sup> ( $\times 10^3$ )
La	1046.26	619.82	3.90	11.10	1411.18	879.93
Ce	43.56	61.63	3.43	11.60	105.98	76.63
Pr	729.59	396.08	2.79	10.60	1466.22	925.68
Nd	648.74	342.18	2.52	8.81	1377.98	913.76
Sm	525.21	275.32	3.50	11.90	1189.66	821.55
Eu	419.36	225.40			97.30	708.11
Gd	400.60	217.42	3.74	14.30	1149.53	757.01
Tb	243.31	132.30			930.82	618.24
Dy	143.05	81.60	5.02	17.60	785.26	525.64
Y	73.73	45.64			765.43	458.55
Ho	91.04	55.98			710.53	476.32
Er	56.99	38.21	7.93	25.2	737.13	500.00
Tm					765.16	534.19
Yb	24.82	19.04	8.72	28.8	846.48	582.09
Lu	18.70	15.12			975.61	667.68
Nd/Yb <sup>*</sup>	26.14	17.97	0.29	0.31	1.63	1.57

<sup>a</sup>Lake Eyasi stromatolite data from Table 3 normalized to ELW. Samples 1-10 are averaged after normalization.

<sup>b</sup>Cuatro Ciénegas data from Table 14.3 of Johannesson et al. [2014].

<sup>c</sup>Nakabusa hot spring microbialite data is calculated using Table 1 of Takahashi et al. [2005]. Sample 1 originates from sulfate reducing bacteria, whereas sample 2 comes from phototrophic bacteria.

\*Note that this is Nd/Yb, not Yb/Nd. This represents LREE (not HREE) enrichment.

Two additional studies normalize the REY signatures of terrestrial microbialites to those of their ambient water. Johannesson et al. [2014] investigates stromatolites from the Cuatro Ciénegas bolson in Coahuila, Mexico, while Takahashi et al. [2005] analyzes microbialites from the Nakabusa hot spring in Japan. Neither of the aforementioned studies show uniformly flat ambient water normalized REY patterns. Table 4 compares the partition/distribution coefficients calculated in this study to those provided by Johannesson et al. [2014] and Takahashi et al. [2005]. The Nd/Yb ratio is also provided to quantify LREE enrichment or depletion, relative to the ambient water, and clearly indicates that each of these these terrestrial microbialites fractionate REEs.

Like the Lake Eyasi stromatolites, the Nakabusa hot spring microbialites were formed under alkaline conditions, at pH  $\gtrsim 8$  (Takahashi et al. 2005). As seen in Figure 4a of Takahashi et al. [2005], the water normalized REY patterns are enriched in LREEs and display negative Ce and Eu anomalies. Takahashi et al. [2005, 2007] demonstrate that the functional groups on bacterial cell surfaces preferentially sorb HREEs compared to other REEs. Takahashi et al. [2005] contributes the relative LREE enrichment of natural

microbialites, counter to his lab results, to alkaline thermal conditions. Takahashi et al. [2005] reasons that according to van Middlesworth and Wood [1998], in alkaline thermal conditions, the prevailing speciation of REEs in the aqueous phase is as strong carbonate and hydroxide complexes. These complexes are subsequently able to out-compete bacterial surface functional groups and EPS for HREEs, as REE stability constants increase with atomic number along the series for both hydroxyl and carbonate ions (Quinn et al. 2004; Liu and Byrne 1998; Luo and Byrne 2004). Takahashi et al. [2005] concludes that the decreased availability of HREEs to complex with bacterial cell surfaces in solution, resulted in the appearance of microbialite bacteria to preferentially incorporate LREEs from the ambient water.

The Cuatro Ciéegas stromatolites were formed in neutral pH (mean 7.2) and are enriched in HREEs (Johannesson et al. 2014). Johannesson et al. [2014] explains this by concluding that the bacterial surface functional groups are able to out-compete the hydroxide complexes as well as the relatively weak sulfate, bicarbonate, and chloride complexes for REEs in neutral pH. Johannesson et al. [2014] tests the theory to determine if adsorption to the bacterial cell wall is the primary mechanism for REE uptake in the stromatolite. Johannesson et al. [2014] utilizes the partition coefficients ( $K_d$ ) for REE adsorption onto cell walls at pH 4 given by Takahashi et al. [2007]. Since  $K_d = [\text{REE}]_{\text{solid}} / [\text{REE}]_{\text{solution}}$ , Johannesson et al. [2014] is able to normalize  $[\text{REE}]_{\text{solid}}$  to  $K_d \times [\text{REE}]_{\text{solution}}$  in order to determine the extent to which bacterial surfaces take up REEs. Whereby if the resulting pattern is flat, it indicates that bacterial surfaces are the primary mechanism for REE uptake in the stromatolite. The resulting Figure 14.10 of Johannesson et al. [2014] (which shows patterns near 1) indicates that surface functional groups played a strong role in REE uptake, and it is suggested that the minor HREE enrichment depicted could be caused by REE complexation by other organic ligands such as EPS or biofilms.

In addition to plotting the REY concentrations normalized to the measured ambient water REY concentrations, Takahashi et al. [2005] and Johannesson et al. [2014] normalize microbialite REY concentrations to solution complexation corrected water concentrations, removing the REY complexed to hydroxide and carbonate complexes, respectively. This provides a more accurate representation of REY fractionation with respect to the ambient water, considering that REYs held within strong carbonate and hydroxide complexes are made unavailable for uptake by cell surfaces.

In the case of the Lake Eyasi stromatolites, the explanation provided by Takahashi et al. [2005] for water normalized LREE enrichment is possible. Though Lake Eyasi is not a thermal alkaline lake, alkaline lakes are typically dominated by carbonate complexes which preferentially complex HREEs relative to LREEs (Johannesson et al. 1994). Although, the fractionation of REEs demonstrated by the Lake Eyasi stromatolite is orders of magnitude stronger than that displayed by the Nakabusa microbialites, as evident by a comparison of their respective Nd/Yb ratios in Table 4. The increased alkalinity of Lake Eyasi ( $\text{pH} > 9$  as opposed to  $\text{pH} \gtrsim 8$ ) could be the reason for the increased relative LREE enrichment, due to the potentially increased presence of carbonate which dominates REE complexation (Möller and Bau 1993). The theoretically increased amount of carbonate complexes in the alkaline lake would subsequently lead to an enrichment of Ce and HREEs complexed in solution and thus a depletion of Ce and HREEs available for EPS adsorption (Möller

and Bau 1993). This then results in the appearance of the stromatolites to preferentially sorb LREEs. Nonetheless, it seems unlikely that this effect would be of the magnitude that it appears. Normally, an LREE enrichment in a carbonate could be contributed to the presence of clay or secondary iron oxyhydroxides (Takahashi et al. 2005), however the possibility of contamination by an aluminosilicate phase has already been discounted.

#### 4.4.2 Terrigenous Normalization

There is, however, another more plausible explanation as to the origin of the Lake Eyasi stromatolite's REY signatures. The Lake Eyasi water is visibly dirty, with a relatively high TSS (total suspended solid) value of around 80 mg/L. In Figure 7, it is clear that there is a large difference between the filtered water and the filter material, in both concentration and shale-normalized REY pattern. This indicates that REYs in lake Eyasi are transported in both ionic/colloidal phases and particulate phases. Agglutinated (and fenestral) stromatolites, like the Lake Eyasi stromatolite, are known to form from the trapping and binding of detrital sediment (Riding 1991). According to the study by Suarez-Gonzalez et al. [2019], the following four requirements must be satisfied for trapping and binding to play a significant role in sedimentation:

1. Grains are present and available.
2. Sufficient water agitation to supply the microbialite with grains.
3. High electrolyte concentrations to increase EPS adhesiveness (i.e. saline conditions).
4. Low  $\text{CaCO}_3$  saturation state as to not trigger early precipitation within the EPS, hindering the trapping and binding process.

Continental hyper-saline lakes are known to satisfy each of these conditions, with the exception of condition 4 due to their high alkalinity (Suarez-Gonzalez et al. 2019). However, soda lakes along the East African Rift System, like Lake Eyasi, contain low concentrations of Ca, with increased concentrations during the wet season and decreased concentrations during the dry season (Deocampo and Renaut 2016). Regarding Ca, generally low concentrations accompanied by seasonal variations could provide the perfect environment for stromatolites to trap and bind sediment without  $\text{CaCO}_3$  supersaturation. The Lake Eyasi stromatolites match the description for an agglutinated stromatolite formed by trapping and binding mechanisms. This hypothesis could be further supported by the previously discussed correlation between REYs and Th, though this is dependant on the solution complexation within Eyasi waters. If this is true, then the REY pattern normalized In Figure 8a should be flat, however it is not.

It is clear that there are two distinct mineral phases depicted in Figure 8a. The stromatolites, samples 1-10, are calcium carbonate in the form of calcite (See fig A.2). The stromatolite is finely grained and gray in color. On the contrary, the pore material, sample 11, is different in almost every way. Sample 11 is not a carbonate, it is course grained,

and reddish orange in color. In addition to its unique REY signature, the major element composition is also very different. It contains particularly high concentrations of Al and Fe, characteristic of minerals so orange. Agglutinated stromatolites trap and bind small, likely micritic, particles while organic filaments conquer them. However, they are unable to colonize coarse grains because they are simply too large for the EPS to retain (Riding 1991). The Lake Eyasi stromatolites likely preferentially incorporated micritic particles from the water to form its good wrinkly lamination through episodic sedimentation during times of microbial growth. When fenestrae inevitably developed for the same reason lamination is wrinkled (that being the stromatolites position in a seasonal lake margin), un-colonized detritus remained in the fenestrae. Within the fenestrae, any remaining micrite particles were likely colonized, leaving only the coarse grains leftover. Note that these grains were not trapped, rather deposited. Since ELF represents all particulate matter in the water  $> 2\mu m$ , its REY signature represents a combination of all the detritus suspended in the water column. To test this hypothesis, the values of the stromatolite and the pore material are averaged and subsequently normalized to ELF (Figure 11). If the resulting pattern is flat around a value of 1, that suggests that the stromatolite formed by a process of trapping and binding.

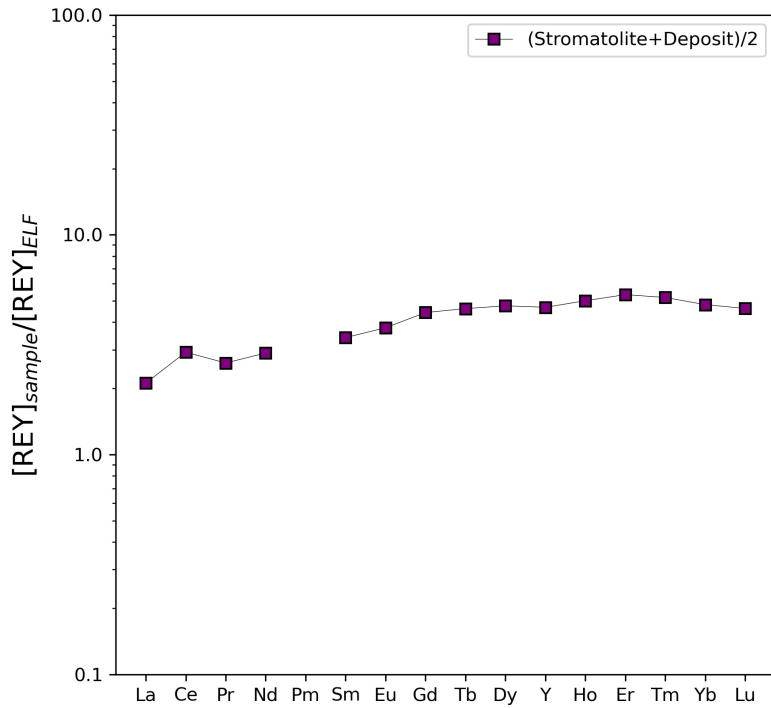


Figure 11: The mean values of samples 1-10 are averaged with those of sample 11 and subsequently normalized to ELF.

The pattern seen in Figure 11 is naturally flatter than the pattern displayed by sample 11, and less flat than samples 1-10 (when normalized against ELF). The ELF normalized Yb/Nd ratios for samples 1-10, sample 11, and the resulting pattern are 1.417, 1.989, and

1.659, respectively. What is not reflected by the Yb/Nd ratios is how the Ce anomalies are lessened in the resulting pattern to merely a minor positive Ce anomaly, which supports the hypothesis. There is some HREE enrichment and a discernible M-type tetrad effect for Gd–Tb–Dy–Ho and Er–Tm–Yb–Lu. The tetrad effect is a phenomena observed in REEs due to the increasing stability accompanying subsequent filling of the 4f electron shell across four groups of elements in the series (Peppard et al. 1969).

Trapping and binding alone is not enough to produce lamination, this process must be periodically interrupted to allow for bioinduced precipitation of a micritic lamina (Dupraz et al. 2009; Suarez-Gonzalez et al. 2019). This event occurs during a periods of low accretion, while the outer micritic lamina is precipitated simultaneously the biofilm (which has colonized the trapped and bound grains) is lithified (Suarez-Gonzalez et al. 2019). The lithification occurs through the precipitation of clotted-peloidal micrite likely due to the influence of degradation of the EPS by heterotrophic bacteria. The bioinduced precipitation of micrite from the ambient water to form layers may be the key to the HREE enrichment in Figure 11. It has already been established that microbial communities preferentially sorb HREEs during microbialite precipitation (Takahashi et al. 2005; Takahashi et al. 2007). This is further supported by observations from Johannesson et al. [2014], a study which actually confirms that their microbialite is **not** formed by trapping and binding since the ambient water does not transport REEs in the particulate phase. The intermittent precipitation could be the reason for the input-normalized fractionation between light and heavy REEs depicted in Figure 11.

One interesting relationship observed was that when sample 11 is normalized against the average of the stromatolite and ELF, the resulting pattern is almost uniformly at 1, with the exception of a positive Ce anomaly (See Fig A.1 in the Appendix). This could hold the key to the origin of the deposited material (sample 11). Continuing on the theory that the stromatolite was formed by trapping and binding, this would be indicative that ELF contains a multiplicity of minerals not deposited in the fenestrae of the stromatolite nor trapped by the stromatolite itself. This would also imply the presence of an unknown mineral containing a positive Ce anomaly within the detritus. This system is even more difficult to interpret when taking into account the Mg-rich clay minerals which form due to microbial decay in Lake Eyasi (Deocampo 2005), which could increase fractionation by incorporating the less soluble  $\text{Ce}^{4+}$ .

## 5 Conclusions

The formation process of the Lake Eyasi thrombotic-stromatolites remains uncertain. It is concluded that despite different morphologies within the individual microbialites, the major and trace element concentrations are almost identical. This indicates that the general formation process remained the same throughout its lifetime, with minor variations likely due to the impact of environmental changes on microbial communities. For future studies regarding REY signatures in biogenic carbonate matrices, a 0.5 M HNO<sub>3</sub> leaching is sufficient. Any attempt to perform a bulk digestion using HF could result in depleted REY concentrations and a false negative Y anomaly.

It is obvious that in order to determine a relationship between a stromatolite's REY pattern and the REY pattern of it's ambient water, a consistent method for differentiation of formation processes must first be developed. In the case of the Lake Eyasi stromatolites, the discussed hypotheses should be further investigated after solution complexation modelling of Lake Eyasi waters. This would provide valuable insights into water chemistry with implications for potential formation processes. If it were to be concluded that the stromatolite was formed authigenically, then it would be clear that terrestrial stromatolites could not be used as REY proxies for their ambient water on the basis that they do not fractionate REYs. The idea that their solid/liquid partition coefficients can be applied to ancient stromatolites to reconstruct ancient REY water chemistry also seems unlikely given the complex system dynamics at play. Whether ancient marine stromatolites can be used as a proxy for seawater REY chemistry or not, if they can be distinguished from their terrestrial counterparts, is beyond the scope of this paper. However, with a better understanding of the mechanistic processes involved in REY discrimination within stromatolites, it could be possible to link the taxonomic functional potential of microbes involved in microbialite formation to certain REY patterns. Further studies should be holistic, investigating not only the geochemistry, but also the biological aspect. Using methods described by White III et al. [2015], it is theoretically possible to uncover the taxonomic functional potential of microbes which formed Holocene-aged, and even ancient stromatolites, if the stromatolite is well enough preserved.

Given the opportunity, an additional method to potentially ascertain if the stromatolites are authigenically precipitated would be to use EPMA (electron probe microanalyzer) to determine if specific layers alternate between sodium carbonates and calcium carbonates seasonally. Due to the nature of soda lakes, sodium carbonates form during the wet season whereas calcium carbonates form during the dry season. If the composition were to alternate between layers, this would be indicative of precipitation from solution. Although, this could prove inconclusive since groundwater input associated with the lake's margin could provide a constant input of cations. Another potentially enlightening analysis could be the use of LA-ICP-MS (laser ablation inductively coupled plasma mass spectrometry) to recognize trace element differences between individual layers of the stromatolite. The differences in color between layers indicate differences in composition which are too small scale for traditional ICP-MS analysis to quantify without spot analyses. A mineralogical analysis using XRD (X-Ray diffraction) or light optical microscopy (e.g., Lencina et al. 2021) analytical methods could also provide relevant information to determine the forma-

tion processes involved.

Whether the stromatolite was formed authigenically or by the trapping and binding of terrigenous sediment, the origin of sample 11 remains unclear. This aspect should be further investigated, particularly with regards to the relationship observed in Figure A.1. The major element composition of sample 11 should also be compared to the major element composition of ELF. The sediment found within the fenestrae of the stromatolite could be a secondary precipitate or deposited material. Further studies should not forgo the potential implications of these pore sediments. Not only should studies continue to investigate their origin and implications, but they should also be careful to avoid the contamination of actual stromatolite/microbialite samples by these minerals.

## References

- Brian Alexander. Trace element analyses in geological materials using low resolution inductively coupled plasma mass spectrometry (icpms). *Jacobs University School of Engineering and Science*, 08 2008.
- Abigail C. Allwood, Malcolm R. Walter, Ian W. Burch, and Balz S. Kamber. 3.43 billion-year-old stromatolite reef from the pilbara craton of western australia: Ecosystem-scale insights to early life on earth. *Precambrian Research*, 158(3):198–227, 2007. ISSN 0301-9268. doi: <https://doi.org/10.1016/j.precamres.2007.04.013>. URL <https://www.sciencedirect.com/science/article/pii/S0301926807001234>. Earliest Evidence of Life on Earth.
- Jean-Alix Barrat, Germain Bayon, Xudong Wang, Samuel Le Goff, Marie-Laure Rouget, Bleuenn Gueguen, and Douraied Ben Salem. A new chemical separation procedure for the determination of rare earth elements and yttrium abundances in carbonates by icp-ms. *Talanta*, 219:121244, 2020. ISSN 0039-9140. doi: <https://doi.org/10.1016/j.talanta.2020.121244>. URL <https://www.sciencedirect.com/science/article/pii/S003991402030535X>.
- J. Casanova. *Stromatolites from the East African Rift: A Synopsis*, pages 193–226. Springer Netherlands, Dordrecht, 1994. ISBN 978-94-011-1124-9. doi: 10.1007/978-94-011-1124-9\_8. URL [https://doi.org/10.1007/978-94-011-1124-9\\_8](https://doi.org/10.1007/978-94-011-1124-9_8).
- Maree Corkeron, Gregory E. Webb, Joshua Moulds, and Kathleen Grey. Discriminating stromatolite formation modes using rare earth element geochemistry: Trapping and binding versus in situ precipitation of stromatolites from the neoproterozoic bitter springs formation, northern territory, australia. *Precambrian Research*, 212-213: 194–206, 2012. ISSN 0301-9268. doi: <https://doi.org/10.1016/j.precamres.2012.04.019>. URL <https://www.sciencedirect.com/science/article/pii/S0301926812001155>.
- J. B. Dawson, H. Pinkerton, D. M. Pyle, and C. Nyamweru. June 1993 eruption of Oldoinyo Lengai, Tanzania: Exceptionally viscous and large carbonatite lava flows and evidence for coexisting silicate and carbonate magmas. *Geology*, 22(9):799–802, 09 1994. ISSN 0091-7613. doi: 10.1130/0091-7613(1994)022<0799:JE0OLT>2.3.CO;2. URL [https://doi.org/10.1130/0091-7613\(1994\)022<0799:JE0OLT>2.3.CO;2](https://doi.org/10.1130/0091-7613(1994)022<0799:JE0OLT>2.3.CO;2).
- Daniel Deocampo. Evaporative evolution of surface waters and the role of aqueous co<sub>2</sub> in magnesium silicate precipitation: Lake eyasi and ngorongoro crater, northern tanzania. *South African Journal of Geology - S Afr J GEOL*, 108:493–504, 12 2005. doi: 10.2113/108.4.493.
- Daniel Deocampo and Robin Renaut. *Geochemistry of African Soda Lakes*, pages 77–93. Springer International Publishing, 08 2016. ISBN 978-3-319-28620-4. doi: 10.1007/978-3-319-28622-8\_4.
- Peter Dulski. Reference materials for geochemical studies: New analytical data by icp-ms and critical discussion of reference values. *Geostandards Newsletter*, 25:87 – 125, 05 2007. doi: 10.1111/j.1751-908X.2001.tb00790.x.

- Christophe Dupraz, R. Pamela Reid, Olivier Braissant, Alan W. Decho, R. Sean Norman, and Pieter T. Visscher. Processes of carbonate precipitation in modern microbial mats. *Earth-Science Reviews*, 96(3):141–162, 2009. ISSN 0012-8252. doi: <https://doi.org/10.1016/j.earscirev.2008.10.005>. URL <https://www.sciencedirect.com/science/article/pii/S0012825208001190>. Microbial Mats in Earth’s Fossil Record of Life: Geobiology.
- H. Elderfield, M. Whitfield, J. D. Burton, M. P. Bacon, and P. S. Liss. The oceanic chemistry of the rare-earth elements [and discussion]. *Philosophical Transactions of the Royal Society of London. Series A, Mathematical and Physical Sciences*, 325(1583):105–126, 1988. ISSN 00804614. URL <http://www.jstor.org/stable/38104>.
- H. J. Hofmann, K. Grey, A. H. Hickman, and R. I. Thorpe. Origin of 3.45 Ga coniform stromatolites in Warrawoona Group, Western Australia. *GSA Bulletin*, 111(8):1256–1262, 08 1999. ISSN 0016-7606. doi: 10.1130/0016-7606(1999)111<1256:OOGCSI>2.3.CO;2. URL [https://doi.org/10.1130/0016-7606\(1999\)111<1256:OOGCSI>2.3.CO;2](https://doi.org/10.1130/0016-7606(1999)111<1256:OOGCSI>2.3.CO;2).
- P. Jakeš and J. Gill. Rare earth elements and the island arc tholeiitic series. *Earth and Planetary Science Letters*, 9(1):17–28, 1970. ISSN 0012-821X. doi: [https://doi.org/10.1016/0012-821X\(70\)90018-X](https://doi.org/10.1016/0012-821X(70)90018-X). URL <https://www.sciencedirect.com/science/article/pii/0012821X7090018X>.
- Karen Johannesson, W. Lyons, and David Bird. Rare earth element concentrations and speciation in alkaline lakes from the western usa. *Geophysical Research Letters*, 21:773–776, 05 1994. doi: 10.1029/94GL00005.
- Karen H. Johannesson, Doyle L. Hawkins, and Alejandra Cortés. Do archean chemical sediments record ancient seawater rare earth element patterns? *Geochimica et Cosmochimica Acta*, 70(4):871–890, 2006. ISSN 0016-7037. doi: <https://doi.org/10.1016/j.gca.2005.10.013>. URL <https://www.sciencedirect.com/science/article/pii/S0016703705008343>.
- Karen H. Johannesson, Katherine Telfeyan, Darren A. Chevis, Brad E. Rosenheim, and Matthew I. Leybourne. *Rare Earth Elements in Stromatolites—1. Evidence that Modern Terrestrial Stromatolites Fractionate Rare Earth Elements During Incorporation from Ambient Waters*, pages 385–411. Springer Netherlands, Dordrecht, 2014. ISBN 978-94-007-7615-9. doi: 10.1007/978-94-007-7615-9\_14. URL [https://doi.org/10.1007/978-94-007-7615-9\\_14](https://doi.org/10.1007/978-94-007-7615-9_14).
- Mustafa Kaya, Belgin Yildirim, Mustafa Kumral, and Ahmet Sasmaz. Trace and rare earth element (ree) geochemistry of recently formed stromatolites at lake salda, sw turkey. *Water*, 15:733, 02 2023. doi: 10.3390/w15040733.
- Wolfgang E. Krumbein, Ulrike Brehm, Gisela Gerdes, Anna A. Gorbushina, George Levit, and Katarzyna A. Palinska. *Biofilm, Biodictyon, Biomat Microbialites, Oolites, Stromatolites Geophysiology, Global Mechanism, Parahistology*, pages 1–27. Springer Netherlands, Dordrecht, 2003. ISBN 978-94-017-0193-8. doi: 10.1007/978-94-017-0193-8\_1. URL [https://doi.org/10.1007/978-94-017-0193-8\\_1](https://doi.org/10.1007/978-94-017-0193-8_1).

- Agustina Lencina, Mariana Soria, Fernando Gomez, Emmanuelle Gérard, and Maria Farías. Composite microbialites: Thrombolite, dendrolite, and stromatolite associations in a modern environment, pozo bravo lake, salar de antofalla, catamarca puna, argentina. *Journal of Sedimentary Research*, 91:1305–1330, 12 2021. doi: 10.2110/jsr.2020.166.
- Xuewu Liu and Robert H. Byrne. Comprehensive investigation of yttrium and rare earth element complexation by carbonate ions using icp–mass spectrometry. *Journal of Solution Chemistry*, 27:803–815, 1998. URL <https://api.semanticscholar.org/CorpusID:91812593>.
- Yu-Ran Luo and Robert H. Byrne. Carbonate complexation of yttrium and the rare earth elements in natural waters1 1associate editor: D. rimstidt. *Geochimica et Cosmochimica Acta*, 68(4):691–699, 2004. ISSN 0016-7037. doi: [https://doi.org/10.1016/S0016-7037\(03\)00495-2](https://doi.org/10.1016/S0016-7037(03)00495-2). URL <https://www.sciencedirect.com/science/article/pii/S0016703703004952>.
- S. M. McLennan. *Chapter 7. RARE EARTH ELEMENTS IN SEDIMENTARY ROCKS: INFLUENCE OF PROVENANCE AND SEDIMENTARY PROCESSES*, pages 169–200. De Gruyter, Berlin, Boston, 1989. ISBN 9781501509032. doi: doi:10.1515/9781501509032-010. URL <https://doi.org/10.1515/9781501509032-010>.
- Peter Möller and Michael Bau. Rare-earth patterns with positive cerium anomaly in alkaline waters from lake van, turkey. *Earth and Planetary Science Letters*, 117(3):671–676, 1993. ISSN 0012-821X. doi: [https://doi.org/10.1016/0012-821X\(93\)90110-U](https://doi.org/10.1016/0012-821X(93)90110-U). URL <https://www.sciencedirect.com/science/article/pii/0012821X9390110U>.
- D F Peppard, G W Mason, and S Lewey. A tetrad effect in the liquid–liquid extraction ordering of lanthanides(iii). *J. Inorg. Nucl. Chem.*, 31: 2271-2(July 1969)., 1 1969. doi: 10.1016/0022-1902(69)90044-X. URL <https://www.osti.gov/biblio/4757028>.
- Kelly Quinn, Robert Byrne, and Johan Schijf. Comparative scavenging of yttrium and the rare earth elements in seawater: Competitive influences of solution and surface chemistry. *Aquatic Geochemistry*, 10:59–80, 03 2004. doi: 10.1023/B:AQUA.0000038959.03886.60.
- Robert Riding. *Calcareous Algae and Stromatolites*, chapter Classification of Microbial Carbonates, pages 21–51. Springer Berlin, Heidelberg, 01 1991. ISBN 978-3-642-52337-3. doi: 10.1007/978-3-642-52335-9\_2.
- Robert Riding. Microbialites, stromatolites, and thrombolites. *Encyclopedia of Geobiology*, pages 635–654, 01 2011. doi: 10.1007/978-1-4020-9212-1\_196.
- Hugh Rollinson. Using geochemical data: Evolution, presentation, interpretation. *Longman Scientific and Technical Press*, 26, 01 1995.
- E. Rongemaille, G. Bayon, C. Pierre, C. Bollinger, N.C. Chu, Y. Fouquet, V. Riboulot, and M. Voisset. Rare earth elements in cold seep carbonates from the niger delta. *Chemical Geology*, 286(3):196–206, 2011. ISSN 0009-2541. doi: <https://doi.org/10.1016/j.chemgeo.2011.05.001>. URL <https://www.sciencedirect.com/science/article/pii/S0009254111001884>.

- Katharina Schier, Tobias Himmller, Aivo Lepland, Dennis Kraemer, Jasmin Schönenberger, and Michael Bau. Insights into the rey inventory of seep carbonates from the northern norwegian margin using geochemical screening. *Chemical Geology*, 559:119857, 2021. ISSN 0009-2541. doi: <https://doi.org/10.1016/j.chemgeo.2020.119857>. URL <https://www.sciencedirect.com/science/article/pii/S000925412030396X>.
- P. Suarez-Gonzalez, M.I. Benito, I.E. Quijada, R. Mas, and S. Campos-Soto. ‘trapping and binding’: A review of the factors controlling the development of fossil agglutinated microbialites and their distribution in space and time. *Earth-Science Reviews*, 194:182–215, 2019. ISSN 0012-8252. doi: <https://doi.org/10.1016/j.earscirev.2019.05.007>. URL <https://www.sciencedirect.com/science/article/pii/S0012825218307293>.
- Yoshio Takahashi, Xavier Châtellier, Keiko H. Hattori, Kenji Kato, and Danielle Fortin. Adsorption of rare earth elements onto bacterial cell walls and its implication for ree sorption onto natural microbial mats. *Chemical Geology*, 219(1):53–67, 2005. ISSN 0009-2541. doi: <https://doi.org/10.1016/j.chemgeo.2005.02.009>. URL <https://www.sciencedirect.com/science/article/pii/S0009254105000926>.
- Yoshio Takahashi, Taeko Hirata, Hiroshi Shimizu, Takuo Ozaki, and Danielle Fortin. A rare earth element signature of bacteria in natural waters? *Chemical Geology*, 244(3): 569–583, 2007. ISSN 0009-2541. doi: <https://doi.org/10.1016/j.chemgeo.2007.07.005>. URL <https://www.sciencedirect.com/science/article/pii/S0009254107003269>.
- Martin J. Van Kranendonk, Gregory E. Webb, and Balz S. Kamber. Geological and trace element evidence for a marine sedimentary environment of deposition and biogenicity of 3.45 ga stromatolitic carbonates in the pilbara craton, and support for a reducing archaean ocean. *Geobiology*, 1(2):91–108, 2003. doi: <https://doi.org/10.1046/j.1472-4669.2003.00014.x>. URL <https://onlinelibrary.wiley.com/doi/abs/10.1046/j.1472-4669.2003.00014.x>.
- Paul E. van Middlesworth and Scott A. Wood. The aqueous geochemistry of the rare earth elements and yttrium. part 7. ree, th and u contents in thermal springs associated with the idaho batholith. *Applied Geochemistry*, 13(7):861–884, 1998. ISSN 0883-2927. doi: [https://doi.org/10.1016/S0883-2927\(98\)00019-5](https://doi.org/10.1016/S0883-2927(98)00019-5). URL <https://www.sciencedirect.com/science/article/pii/S0883292798000195>.
- Gregory Webb and Balz Kamber. Webb, g. e. & kamber, b. s. rare earth elements in holocene reefal microbialites: a new shallow seawater proxy. *geochim. cosmochim. acta* 64, 1557-1565. *Geochimica et Cosmochimica Acta*, 64:1557–1565, 05 2000. doi: 10.1016/S0016-7037(99)00400-7.
- Richard White III, Ian Power, Greg Dipple, Gordon Southam, and Curtis Suttle. Metagenomic analysis reveals that modern microbialites and polar microbial mats have similar taxonomic and functional potential. *Frontiers in Microbiology*, 6, 09 2015. doi: 10.3389/fmicb.2015.00966.
- Erik Östhols. Some processes affecting the mobility of thorium in natural ground waters. *Department of Chemistry, Royal Institute of Technology*, 4 1994.

## Appendix

### Figures

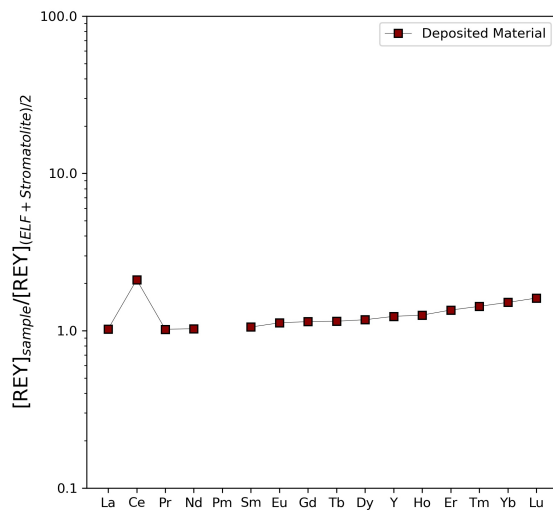


Figure A.1: The averages of samples 1-10 were subsequently averaged with ELF data. The resulting REY data was used as a normalization for sample 11. The plot is almost uniformly at 1, with the exception of a Ce anomaly.

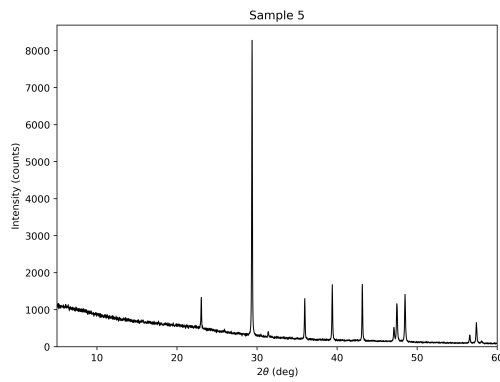


Figure A.2: Raw (unfiltered) XRD data for sample 5. Data is provided by Dr. F. Wilke from the GFZ. The peaks are characteristic of a calcite mineral.

**OES Data**Table A.1: Major element data from the HCl+HNO<sub>3</sub>+HF bulk digestion (Sample#\_Job#).

mg/kg	68_S1	68_S2	68_S3	68_S4	68_S5	14_S11
Al	2789.6	2825.7	6306.2	3305.5	2276.4	49504.1
Ca	212803.8	204359.8	201219.3	201583.1	199224.8	134604.2
Fe	1969.6	2184.6	5390.9	2868.3	2163.2	41371.6
K	744.0	723.0	1194.1	837.8	703.8	11627.6
Mg	3926.3	3855.9	4307.3	4029.6	4002.6	12345.0
Mn	661.0	569.0	1280.2	535.9	495.0	1263.9
Na	8227.5	7920.1	9807.0	8125.1	7301.3	35526.7
Sr	4878.72	4552.61	4196.11	4804.21	5028.76	2614.03

Table A.2: Major element data from the 5 M HNO<sub>3</sub> leaching (Sample#\_Job#).

	78_S1	78_S2	78_S3	78_S4	78_S5
Al	2601.9	3256.7	5881.4	3478.7	2902.4
Ca	286928.0	351007.4	328827.0	350237.7	351756.0
Fe	1093.9	1555.7	3272.5	2051.2	1521.9
K	265.5	355.1	582.2	394.4	363.1
Mg	4017.0	5078.1	5224.1	5486.1	5222.2
Mn	546.6	569.5	1276.9	553.2	519.4
Na	7324.1	8718.3	10339.6	8852.6	8280.2
Sr	6005.55	7084.38	6567.21	7602.52	7664.40

Table A.3: Major element data from the 5% CH<sub>3</sub>COOH acetic acid leaching (Sample#\_Job#).

mg/kg	80_S1	80_S2	80_S3	80_S4	80_S5
Al	1974.6	2065.5	2843.8	2341.1	1943.1
Ca	312564.2	378478.7	359621.2	370411.6	375625.6
Fe	260.6	394.8	458.8	351.8	253.4
K	30.6	111.8	106.0	69.9	-
Mg	4358.4	4583.3	4425.8	4682.3	4518.4
Mn	646.6	551.6	1194.3	523.7	501.0
Na	7521.5	8679.3	8819.5	8741.5	8209.0
Sr	6663.33	6781.55	6224.28	7212.20	7742.08

Table A.4: Major element data from the 0.5 M HNO<sub>3</sub> leaching (Sample#\_Job#).

mg/kg	06_S2	06_S3	06_S4	06_S5
Al	2877.5	5328.9	3039.3	2657.3
Ca	346041.7	312521.4	341686.0	349967.2
Fe	910.9	1478.1	950.5	821.9
K	186.2	265.9	172.4	167.0
Mg	4862.5	4816.7	5206.4	5106.1
Mn	563.3	1236.4	525.4	535.4
Na	8353.7	9599.7	8591.7	7816.6
Sr	6873.46	6057.57	7294.58	7601.27

mg/kg	12_S6	12_S7	12_S9	12_S10	12_S11
Al	-	-	-	-	18577.5
Ca	339294.8	376829.7	359419.7	364483.7	119176.2
Fe	-	-	-	-	5002.5
K	-	-	-	-	793.1
Mg	5108.6	5080.5	4824.0	4880.1	4116.0
Mn	1604.6	302.0	531.6	828.8	718.6
Na	-	-	-	-	23453.3
Sr	5003.29	5770.34	6055.19	6724.59	2430.21

**ICP-MS Data**

Table A.5: ICP-MS CRM Bean Data

Element	Certified Value (mg/kg)	Measured Value (mg/kg)	Measured/Reference Value (%)	Measured Value RSD (%)
La	2.0280	1.915	94	93
Ce	0.7860	0.765	97	102
Pr	0.2820	0.277	98	127
Nd	1.2370	1.201	97	75
Sm	0.2560	0.255	99	73
Eu	0.0676	0.074	110	323
Gd	0.3780	0.386	102	142
Tb	0.0551	0.053	96	306
Dy	0.3600	0.359	100	168
Y	5.3730	4.712	88	86
Ho	0.0849	0.080	94	99
Er	0.2410	0.239	99	249
Yb	0.1730	0.172	100	264
Lu	0.0254	0.024	96	504

Table A.6: Trace element data from the HCl+HNO<sub>3</sub>+HF bulk digestion (Sample#\_Job#).

mg/kg	S1_68	S2_68	S3_68	S4_68	S5_68	14_23_S11
Li	2.29	2.27	3.22	2.64	2.65	19.43
Be	0.10	0.10	0.24	0.15	0.11	2.04
Sc	1.65	1.36	2.64	1.29	0.98	9.97
Ni	7.39	8.82	23.60	12.83	8.82	197.45
Sr	4878.72	4552.61	4196.11	4804.21	5028.76	2614.03
Y	68.11	66.25	91.27	75.03	45.77	112.25
Zr	0.46	0.54	9.32	1.00	0.46	180.54
Nb	2.84	3.62	12.78	5.29	3.77	79.06
Ba	3972.02	3775.11	3268.75	3541.00	3239.92	1632.58
La	192.67	160.60	166.58	141.68	112.40	178.01
Ce	296.90	202.09	284.76	196.71	144.92	560.05
Pr	41.98	36.97	37.47	34.45	27.14	38.77
Nd	155.18	140.00	140.40	133.50	106.19	142.39
Sm	27.07	25.15	25.96	25.05	19.21	26.41
Eu	6.32	5.88	6.12	6.04	4.64	6.59
Gd	25.13	23.62	24.69	24.73	18.96	25.65
Tb	3.37	3.25	3.45	3.47	2.61	3.65
Dy	18.28	18.18	19.64	19.89	14.59	21.20
Ho	3.36	3.40	3.70	3.81	2.75	4.22
Er	9.03	9.49	10.42	10.36	7.37	12.43
Tm	1.08	1.14	1.33	1.24	0.84	1.66
Yb	5.82	6.19	7.59	6.48	4.24	10.08
Lu	0.75	0.81	0.99	0.82	0.54	1.37
Pb	47.09	44.27	37.41	53.49	55.11	36.77
Th	0.34	0.44	3.08	0.99	1.46	104.21
U	0.39	0.49	1.32	0.38	0.26	2.33

Table A.7: Trace element data from the 5 M HNO<sub>3</sub> leaching (Sample#\_Job#).

	mg/kg	S1_78	S2_78	S3_78	S4_78	S5_78						
Li	1.74	2.31	3.19	2.89	2.73		Li	0.57	0.66	0.66	0.46	0.48
Be	0.11	0.14	0.25	0.15	0.12		Be	0.05	0.06	0.09	0.04	0.04
Sc	0.71	1.22	2.01	1.37	1.40		Sc	0.92	1.01	2.13	1.13	1.44
Ni	2.67	3.43	6.45	4.56	3.90		Ni	1.41	1.55	1.91	1.53	1.54
Sr	6005.55	7084.38	6567.21	7602.52	7664.40		Sr	6663.33	6781.55	6224.28	7212.20	7742.08
Y	128.44	161.97	147.54	175.52	170.32		Y	134.55	145.74	130.21	157.95	163.24
Zr	1.25	1.67	4.42	2.83	2.58		Zr	0.31	0.35	0.29	0.31	0.31
Nb	0.23	0.41	0.92	0.76	0.51		Nb	0.01	0.01	0.03	0.02	0.01
Ba	3963.11	4848.45	4038.96	4800.56	4379.93		Ba	4346.21	4480.93	3656.65	4038.72	3975.75
La	263.67	275.15	263.06	247.40	235.45		La	271.12	246.19	233.12	217.95	220.13
Ce	413.77	342.23	407.61	338.85	313.78		Ce	425.07	307.55	350.64	295.05	289.40
Pr	57.70	63.72	59.49	60.24	56.99		Pr	60.48	57.52	52.01	53.17	53.51
Nd	208.16	234.30	216.67	225.06	214.97		Nd	222.42	215.09	194.37	204.46	207.39
Sm	37.87	43.46	39.54	42.98	41.73		Sm	40.33	39.96	35.74	39.63	40.40
Eu	8.88	10.30	9.38	10.46	10.10		Eu	9.49	9.51	8.43	9.54	9.95
Gd	35.13	40.74	37.15	42.79	41.24		Gd	37.23	37.53	33.51	38.96	39.65
Tb	4.82	5.72	5.19	6.24	6.01		Tb	5.03	5.24	4.64	5.64	5.69
Dy	26.20	32.47	29.23	35.22	34.47		Dy	27.77	29.55	26.03	32.12	32.86
Ho	4.80	6.05	5.45	6.56	6.36		Ho	5.06	5.55	4.89	6.06	6.13
Er	12.99	16.85	15.21	18.19	17.51		Er	13.81	15.40	13.69	16.50	16.50
Tm	1.63	2.11	1.93	2.26	2.12		Tm	1.70	1.90	1.71	2.03	2.01
Yb	9.10	12.09	11.21	12.47	11.82		Yb	9.58	10.91	9.93	11.17	11.03
Lu	1.15	1.53	1.44	1.54	1.46		Lu	1.22	1.39	1.28	1.40	1.38
Pb	39.82	45.05	39.59	57.92	59.34		Pb	38.62	36.38	24.51	44.41	50.00
Th	53.74	74.22	69.31	82.75	73.83		Th	23.67	29.35	21.50	33.30	29.71
U	0.27	0.43	1.11	0.33	0.23		U	0.25	0.28	0.70	0.25	0.20

Table A.8: Trace element data from the 5% CH<sub>3</sub>COOH acetic acid leaching (Sample#\_Job#).

Table A.9: Trace element data from the 0.5 M HNO<sub>3</sub> leaching (Sample#-Job#).

mg/kg	S1_06	S2_06	S3_06	S4_06	S5_06	S7_12	S8_12	S9_12	S10_12	S11_12
Li	1.90	1.94	2.08	2.18	2.22	2.03	1.97	2.07	2.82	9.43
Be	0.07	0.10	0.16	0.08	0.08	0.09	0.09	0.11	0.13	0.51
Sc	3.08	3.25	6.14	3.50	3.38	2.47	2.79	2.93	3.60	13.21
Ni	4.02	2.27	3.53	2.80	2.54	4.12	24.71	5.45	5.47	56.02
Sr	7053.55	6873.46	6057.57	7294.58	7601.27	5770.34	6386.53	6055.19	6724.59	2430.21
Y	150.17	155.43	135.50	169.44	167.88	176.70	182.20	156.68	170.19	98.69
Zr	1.31	1.34	2.43	2.00	2.01	2.33	2.26	2.16	3.33	6.10
Nb	0.11	0.14	0.14	0.16	0.13	0.18	0.17	0.16	0.14	0.13
Ba	4697.99	4231.18	3691.79	4445.16	3953.01	4139.23	4559.09	3860.85	3520.62	1215.95
La	304.21	262.75	244.55	237.96	232.12	230.45	237.71	278.41	303.05	153.61
Ce	477.12	329.74	377.46	324.18	312.75	323.35	299.19	313.44	477.60	511.94
Pr	67.85	61.24	55.15	57.45	56.37	56.70	59.10	64.16	69.24	32.86
Nd	247.14	227.35	202.29	217.15	215.87	216.63	226.74	240.20	258.27	119.47
Sm	44.70	41.71	36.81	41.88	41.68	41.01	44.00	44.43	48.24	22.18
Eu	10.22	9.71	8.59	9.96	9.98	10.07	10.79	10.78	11.55	5.42
Gd	39.74	37.77	33.38	39.86	40.30	39.20	43.01	41.89	45.05	21.43
Tb	5.58	5.36	4.77	5.81	5.91	5.64	6.23	5.92	6.32	3.06
Dy	30.61	30.88	26.98	33.79	34.05	33.09	36.09	32.61	34.92	18.22
Ho	5.65	5.80	5.09	6.36	6.39	6.39	6.70	5.81	6.32	3.65
Er	15.33	16.12	14.18	17.33	17.33	18.12	18.22	15.54	17.10	10.88
Tm	1.89	2.02	1.83	2.15	2.14	2.33	2.27	1.88	2.11	1.47
Yb	10.78	11.55	10.36	11.90	11.77	13.47	12.37	10.48	11.80	8.72
Lu	1.36	1.46	1.34	1.46	1.47	1.73	1.50	1.31	1.46	1.15
Pb	45.09	41.79	35.00	53.16	57.44	34.92	56.53	52.90	60.80	25.11
Th	61.21	69.30	59.29	76.78	72.60	81.76	74.59	58.58	69.04	90.17
U	0.30	0.40	0.94	0.30	0.22	0.31	0.21	0.24	0.32	0.94